CDDpress

www.nature.com/cdd

ARTICLE

Check for updates

Sensing of mitochondrial DNA by ZBP1 promotes RIPK3-mediated necroptosis and ferroptosis in response to diquat poisoning

Kunmei Lai[1,2,3,4,8], Junjie Wang[1,2,3,8], Siyi Lin[1,2,3,8], Zhimin Chen[1,2,3], Guo Lin[5], Keng Ye[1,2,3], Ying Yuan[1,2,3], Yujiao Lin[1,2,3], Chuan-Qi Zhong[6], Jianfeng Wu[7✉], Huabin Ma[4✉] and Yanfang Xu[1,2,3,4✉]

Diquat (DQ) poisoning is a severe medical condition associated with life-threatening implications and multiorgan dysfunction. Despite its clinical significance, the precise underlying mechanism remains inadequately understood. This study elucidates that DQ induces instability in the mitochondrial genome of endothelial cells, resulting in the accumulation of Z-form DNA. This process activates Z-DNA binding protein 1 (ZBP1), which then interacts with receptor-interacting protein kinase 3 (RIPK3), ultimately leading to RIPK3-dependent necroptotic and ferroptotic signaling cascades. Specific deletion of either *Zbp1* or *Ripk3* in endothelial cells simultaneously inhibits both necroptosis and ferroptosis. This dual inhibition significantly reduces organ damage and lowers mortality rate. Notably, our investigation reveals that RIPK3 has a dual role. It not only phosphorylates MLKL to induce necroptosis but also phosphorylates FSP1 to inhibit its enzymatic activity, promoting ferroptosis. The study further shows that deletion of mixed lineage kinase domain-like (*Mlkl*) and the augmentation of ferroptosis suppressor protein 1 (FSP1)-dependent non-canonical vitamin K cycling can provide partial protection against DQ-induced organ damage. Combining *Mlkl* deletion with vitamin K treatment demonstrates a heightened efficacy in ameliorating multiorgan damage and lethality induced by DQ. Taken together, this study identifies ZBP1 as a crucial sensor for DQ-induced mitochondrial Z-form DNA, initiating RIPK3-dependent necroptosis and ferroptosis. These findings suggest that targeting the ZBP1/RIPK3-dependent necroptotic and ferroptotic pathways could be a promising approach for drug interventions aimed at mitigating the adverse consequences of DQ poisoning.

Cell Death & Differentiation (2024) 31:635–650; https://doi.org/10.1038/s41418-024-01279-5

INTRODUCTION

Diquat (DQ) is a potent broad-spectrum herbicide known for its capacity to induce severe and potentially lethal damage across multiple organ systems [1–3]. Its deleterious effects are primarily attributed to the induction of reactive oxygen species (ROS) within the mitochondrial matrix, culminating in what is commonly referred to as 'oxidative distress' [4–6]. Despite clinical endeavors to mitigate its impact through the administration of antioxidant agents frequently prove ineffective in managing the fatal consequences of DQ exposure. This ineffectiveness may be attributed to the swift activation of downstream signaling cascades triggered by the excessive mitochondrial oxidative stress, ultimately leading to the demise of resident cells within the afflicted tissue. Furthermore, the precise molecular mechanisms underpinning DQ-induced cell death remain an enigmatic puzzle yet to be deciphered.

Mitochondrial ROS initiation of a sequential series of events is well-established, encompassing mitochondrial dysfunction and the subsequent release of mitochondrial DNA (mtDNA) into the cytoplasm [7]. Compelling evidence has underscored the association between mitochondrial dysfunction, mtDNA instability, and programmed cell death pathways such as necroptosis and ferroptosis [8, 9]. Strikingly, it is noteworthy that ROS exerts influence over mtDNA stability because of mtDNA lacking free DNA ends experiences reduced torsional strain during replication and transcription, which potentially promotes a transition from B- to Z-DNA structures [7, 10]. This transition is driven by diminished activities of mitochondrial DNA topoisomerases, particularly DNA topoisomerase I mitochondrial (TOP1MT) and DNA topoisomerase III alpha (TOP3A) [11]. Recent research highlights the pivotal role of Z-DNA binding protein 1 (ZBP1) as a receptor for nuclear Z-DNA [12], double-stranded Z-RNA [13–15], and Z- mtDNA [16, 17]. ZBP1 serves as a

[1]Department of Nephrology, Blood Purification Research Center, the First Affiliated Hospital, Fujian Medical University, Fuzhou 350005, China. [2]Research Center for Metabolic Chronic Kidney Disease, the First Affiliated Hospital, Fujian Medical University, Fuzhou 350005, China. [3]Department of Nephrology, National Regional Medical Center, Binhai Campus of the First Affiliated Hospital, Fujian Medical University, Fuzhou 350212, China. [4]Central Laboratory, the First Affiliated Hospital, Fujian Medical University, Fuzhou 350005, China. [5]Department of Intensive Care Unit, the First Affiliated Hospital, Fujian Medical University, Fuzhou 350005, China. [6]State Key Laboratory of Cellular Stress Biology, School of Life Sciences, Faculty of Medicine and Life Sciences, Xiamen University, Xiamen, Fujian 361102, China. [7]Laboratory Animal Research Center, Xiamen University, Xiamen, Fujian 361102, China. [8]These authors contributed equally: Kunmei Lai, Junjie Wang, Siyi Lin. ✉email: wzqwjf0728@xmu.edu.cn; mahuabin@fjmu.edu.cn; xuyanfang99@hotmail.com

Received: 12 December 2023 Revised: 8 March 2024 Accepted: 11 March 2024
Published online: 16 March 2024

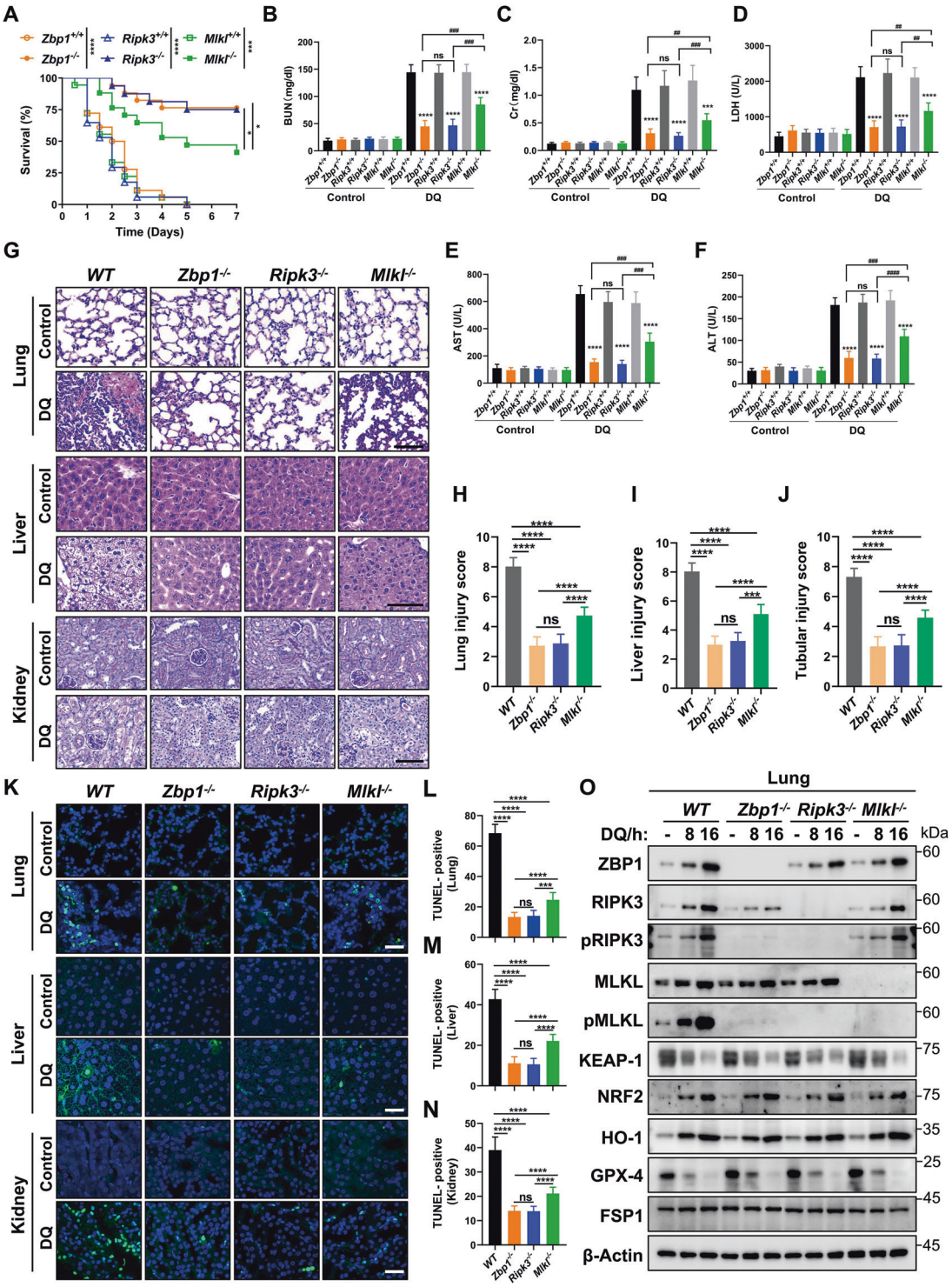

Fig. 1 ZBP1, RIPK3, and MLKL are crucial components for the development of fatal multiple organ injury induced by DQ. The experimental procedure involved treating *Zbp1*$^{-/-}$, *Ripk3*$^{-/-}$, and *Mlkl*$^{-/-}$ and their littermate *wild-type* (*WT*) control mice were subjected to intragastric administration with normal saline or DQ (180 mg/kg). **A** The survival rates of the mice ($n = 13$) were monitored over the specified time period. Blood samples were collected from the mice to measure the levels of various indicators including BUN (Blood Urea Nitrogen) (**B**), Cr (Creatinine) (**C**), LDH (Lactate Dehydrogenase) (**D**), AST (Aspartate Aminotransferase) (**E**), and ALT (Alanine Aminotransferase) (**F**) using the ELISA method ($n = 6$). **G** Representative histological images obtained from lung and liver sections, as well as PAS-stained kidney sections. The scale bar indicates 100 μm. **H**–**J** Histologic scores were assigned to evaluate the extent of lung, liver, and kidney injuries in the respective groups of mice. More than 10 randomly selected fields were assessed for each mouse. $n = 6$. **K** Representative images from TUNEL staining, where green TUNEL-positive cells overlap with blue DAPI-stained nuclei. The magnification was set at 100× and the scale bar represents 50 μm. **L**–**N** Quantification of TUNEL-positive cells in 10 randomly chosen fields for each mouse. $n = 6$. **O** Lung tissues were collected for western blot analysis, focusing on the expression of necroptotic and antioxidant signaling molecules. β-actin was used as a loading control. $n = 4$. $^{*}P < 0.05$, $^{**}P < 0.01$, $^{***}P < 0.001$, $^{****}P < 0.0001$; $^{\#\#}P < 0.01$, $^{\#\#\#}P < 0.001$, $^{\#\#\#\#}P < 0.0001$; ns indicates non-significant results.

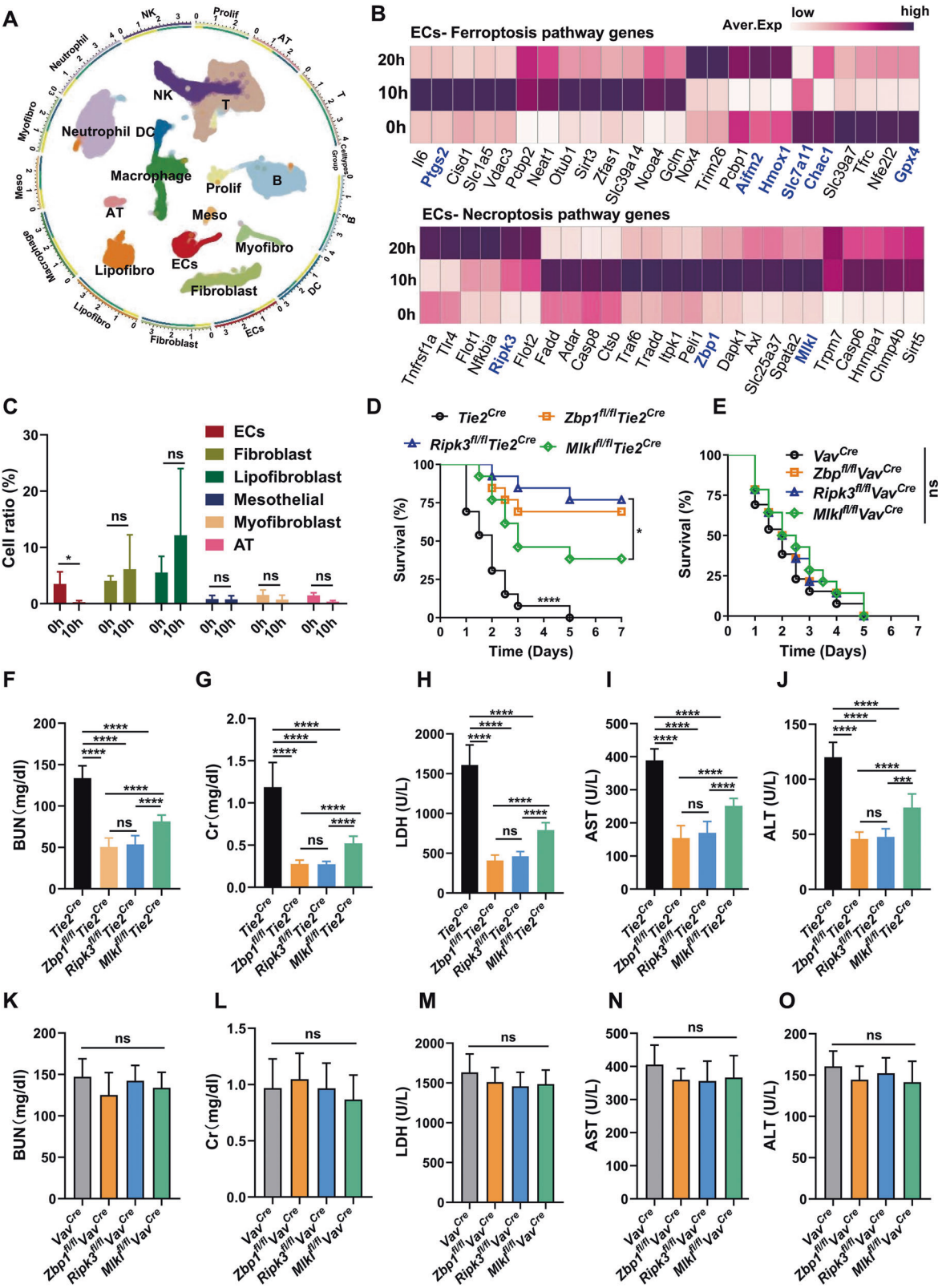

sensor for endogenous Z- nucleic acids, triggering necroptosis through a receptor-interacting protein kinase 3 (RIPK3)-dependent phosphorylation mechanism [18, 19]. It is conceivable that mitochondrial oxidative stress induced by DQ may facilitate the formation of Z-mtDNA, ultimately activating the ZBP1-RIPK3 pathway.

Ferroptosis, a distinctive form of necrotic cell death characterized by lipid peroxidation, provides further insights into the intricate interplay between mitochondrial dysfunction and oxidative stress [20–22]. Critical to the regulation of ferroptosis is ferroptosis suppressor protein 1 (FSP1), which operates through

Fig. 2 Specific deletion of *Zbp1*, *Ripk3*, and *Mlkl* in endothelial cells, rather than hematopoietic cells, provides protection against the fatal multiple organ injury induced by DQ. A–C The mice were subjected to DQ treatment intragastric administration with normal saline or DQ (180 mg/kg) as the time indicated ($n = 3$). Following data quality control, a total of 72,838 high-quality single-cell lung datasets were obtained, with 25,528 cells at 0 h, 30,643 cells at 10 h, and 16,667 cells at 20 h post treatment with diquat. **A** The single-cell sequencing atlas of mouse lung injury induced by diquat at multiple time points (0, 10, 20 h) revealed a total of 13 cell types. AT: alveolar epithelial cells, Prolif: Proliferative cells, Myofibro: Myofibroblasts, ECs: endothelial cells, Lipofibro: Lipofibroblasts, Meso: mesothelial cells, DC: dendritic cells, NK: Natural killer cells. **B** Heatmaps of Necroptosis and Ferroptosis pathway-key genes expressed in lung injury endothelial cells at different time points induced by diquat. **C**. The changes in cell proportions of the six parenchymal cell types at different time points. *$p < 0.05$, ns: non-significant, One-way-ANOVA test. $n = 3$. **D–O** Mice with endothelial cells-specific or hematopoietic cells-specific deficiency of *Zbp1*, *Ripk3*, and *Mlkl* were generated by breeding floxed mice with Tie2-Cre- and Vav-Cre-expressing mice. Subsequently, the mice were subjected to DQ treatment as described in Fig. 1. **D**, **E** The survival rates of these mice ($n = 13$) were monitored over the specified time for both endothelial cells-specific and hematopoietic cells-specific groups. **F–O** Blood samples were collected from the mice to measure the levels of various indicators, including BUN (**F**, **K**), Cr (**G**, **L**), LDH (**H**, **M**), AST (**I**, **N**), and ALT (**J**, **O**) using the ELISA method ($n = 8$). *$P < 0.05$, ***$P < 0.001$, ****$P < 0.0001$; ns denotes non-significant results.

the FSP1-coenzyme Q_{10} (CoQ_{10})-NAD(P)H axis and the vitamin K redox cycle to control lipid peroxides [23–29]. Intriguingly, the observed mitochondrial damage induced by DQ, coupled with the accumulation of lipid ROS due to glutathione depletion, suggests the possibility that DQ may also trigger ferroptosis.

Cells harbor a sophisticated network of tightly regulated cell death pathways that can interconnect and become concurrently activated under specific circumstances, in accordance with the emerging concept of 'PANoptosis' [30, 31]. Research has suggested that the reduction of ROS levels holds promise in mitigating PANoptosis, encompassing various modes of cell demise, including necroptosis, apoptosis, pyroptosis and ferroptosis [32, 33]. The question of whether DQ instigates simultaneous activation of both necroptotic and ferroptotic signaling pathways remains unanswered. A comprehensive investigation is warranted to unravel the intricate interplay between these cell death mechanisms in response to DQ exposure.

Our study presents groundbreaking evidence that exposure to DQ can initiate both necroptotic and ferroptotic pathways, contingent upon the presence of mitochondrial ROS and the formation of Z-mtDNA. We observed that ZBP1 is activated in response to Z-mtDNA, subsequently instigating RIPK3-dependent necroptotic and ferroptotic signaling cascades. Notably, RIPK3 assumes a dual role, phosphorylating MLKL to induce necroptosis and phosphorylating FSP1 to inhibit its enzymatic activity to trigger ferroptosis. The combined deletion of *Mlkl* and the suppression of ferroptosis demonstrated a heightened efficacy in mitigating multiorgan damage induced by DQ. Our findings underscore the promising potential of targeting necroptotic and ferroptotic pathways as prospective therapeutic strategies for ameliorating the severe multiorgan damage associated with DQ.

RESULTS

Deletion of *Zbp1* and *Ripk3* confers protection against DQ-induced lethal organ damage

A comprehensive analysis of gene-deleted mice was conducted to elucidate the involvement of regulated cell death (RCD) in DQ-induced lethal organ damage. Littermate *wild-type* (*WT*) mice were used as controls in all the animal-related experiments. Survival rates were significantly higher in *Zbp1* or *Ripk3* knockout mice, whereas *Mlkl* knockout mice displayed intermediate outcomes (Fig. 1A). Serum levels of indicators for organ injury and cell damage, including AST, ALT, LDH, Scr, and BUN, exhibited significant reductions in $Zbp1^{-/-}$ and $Ripk3^{-/-}$ mice compared to *wild-type (WT)* mice (Fig. 1B–F). Notably, $Zbp1^{-/-}$ and $Ripk3^{-/-}$ mice demonstrated markedly lower serum levels of these indicators in comparison to $Mlkl^{-/-}$ mice (Fig. 1B–F). Histological analysis revealed superior protection against lung, liver, and kidney injuries in $Zbp1^{-/-}$ and $Ripk3^{-/-}$ mice compared to $Mlkl^{-/-}$ mice (Fig. 1G–J). TUNEL staining demonstrated a substantial reduction in the number of apoptotic cells in the lung, liver, and kidney of $Zbp1^{-/-}$ and $Ripk3^{-/-}$ mice compared to $Mlkl^{-/-}$ mice (Fig. 1K–N). Intriguingly, pretreatment with the pan-caspase inhibitor (ZVAD) or the RIPK1 inhibitor (Necrostatin-1, Nec-1) failed to prevent mouse mortality, suggesting that caspases and RIPK1's kinase activity were not essential for DQ-induced lethal organ damage (Fig. S1A). Similarly, GSDMD-mediated pyroptosis was not implicated in DQ-induced organ damage, as the deletion of *Gsdmd* did not influence mouse survival (Fig. S1B).

The protein expression of core components associated with necroptotic and antioxidant pathways in lung, liver, and kidney were assessed following DQ treatment. We observed a significant upregulation of ZBP1, RIPK3, and MLKL, accompanied by a prominent increase in their phosphorylation levels (Figs. 1O and S1C, D). This provides strong confirmation of the pivotal involvement of the ZBP1/RIPK3/MLKL axis in mediating DQ-induced lethal organ damage. Furthermore, the protein level of antioxidant pathway NRF2/HO-1/GPX-4/FSP1 exhibited independent of the ZBP1/RIPK3/MLKL axis, suggesting the existence of an additional mechanism contributing to DQ-induced organ damage (Figs. 1O and S1C, D).

Deletion of *Zbp1* and *Ripk3* in endothelial cells instead of bone marrow-derived cells provided protection against DQ-induced lethal organ damage

Severe damage to the vascular endothelial system easily leads to fatal multiorgan injury [34]. Single-cell RNA sequencing (scRNA-seq) reveals the endothelial cells were the earliest and most significantly affected by diquat among all identified parenchymal cell types (Fig. 2A–C and S2). At the early time point (10 h), the expression of ZBP1, RIPK3, MLKL exhibited significant upregulation alongside with a drastic reduction in lung endothelial cell numbers (Fig. 2B, C, and Fig. S3F–H). The AUCell pathway scoring algorithm were assessed and confirmed the activation of necroptosis pathway (Fig. S3A).

To further investigate the involvement of ZBP1/RIPK3/MLKL-mediated cell death in endothelial cells and hematopoietic cells during DQ-induced organ failure, mice with cell-specific deficiencies in *Zbp1*, *Ripk3*, and *Mlkl* were generated. Consistently, endothelial cell-specific *Zbp1/Ripk3*-deficient mice ($Zbp1^{fl/fl}Tie2^{Cre}$, $Ripk3^{fl/fl}Tie2^{Cre}$) demonstrated enhanced survival rates (Fig. 2D) and exhibited significant protection against lung, liver, and kidney injuries (Fig. 2F–J). Conversely, endothelial cell-specific *Mlkl*-deficient mice ($Mlkl^{fl/fl}Tie2^{Cre}$) displayed intermediate outcomes. Interestingly, hematopoietic cell-specific *Zbp1/Ripk3/Mlkl*-deficient mice ($Zbp1^{fl/fl}Vav^{Cre}$, $Ripk3^{fl/fl}Vav^{Cre}$, $Mlkl^{fl/fl}Vav^{Cre}$) did not demonstrate significant protection (Fig. 2E, K–O). Collectively, these findings suggest that ZBP1/RIPK3/MLKL-mediated cell death in endothelial cells, rather than infiltrating immune cells, predominantly contributes to the progression of DQ-induced multiorgan injury. Of note, endothelial cell-specific deletion of *Zbp1 or Ripk3* displayed better protection than specific deletion of *Mlkl*. Interestingly, single-cell RNA sequencing revealed both necroptosis and ferroptosis pathways were activated in lung endothelial cells after

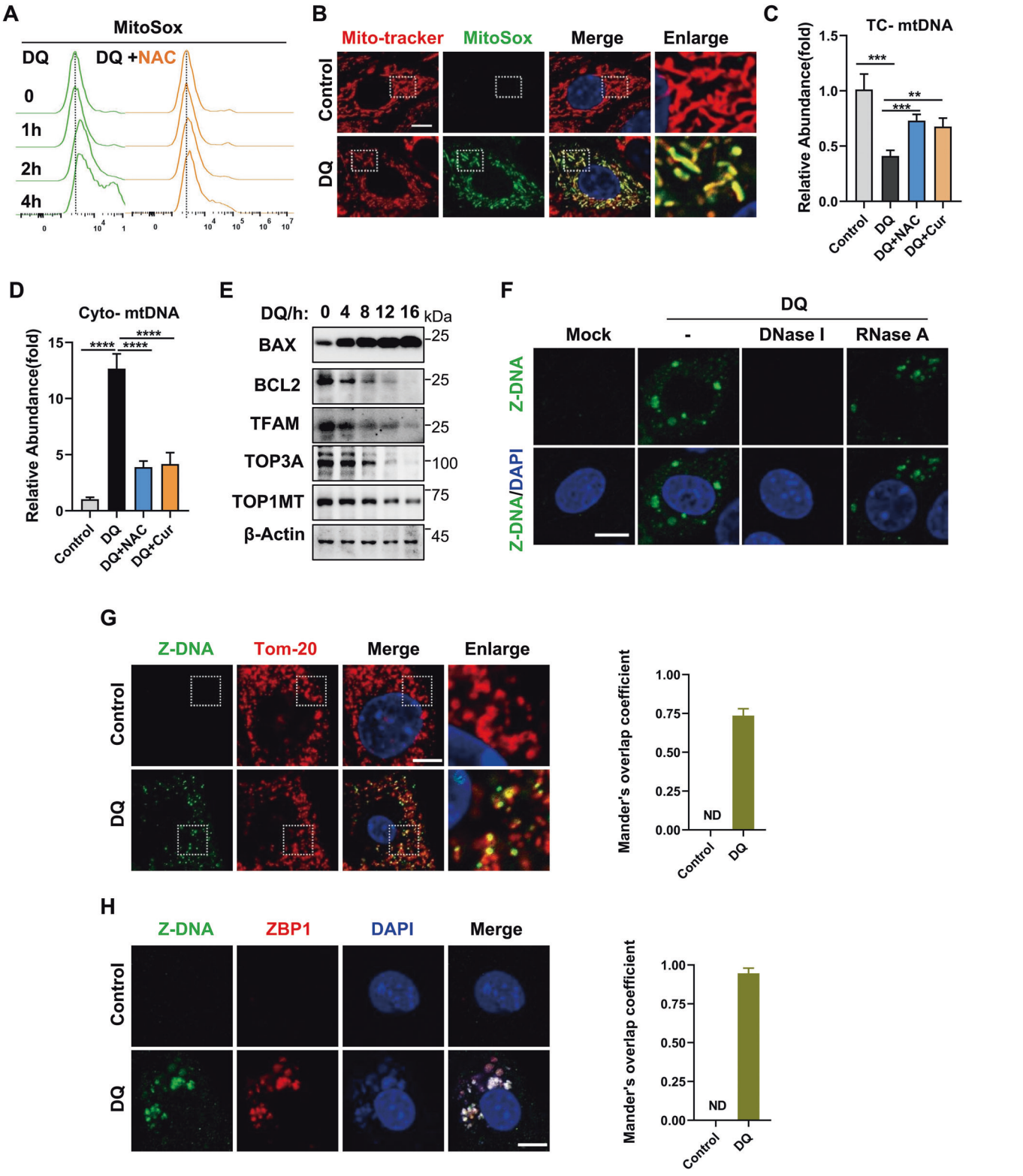

DQ exposure (Figs. 2B and S3), which suggests the existence of ferroptosis potentially contributes to DQ-induced cell death.

DQ induces mitochondrial dysfunction and Z-mtDNA formation

In light of previous studies underscoring mitochondria as the primary target of DQ, we conducted an investigation to ascertain whether DQ-induced cell death operates through mitochondrial pathways. The results revealed mitochondrial fragmentation and a decline in mitochondrial membrane potential (MMP) in endothelial cells (ECs) upon DQ exposure (Fig. S4A and H, I), along with the elevated both cytosolic and mitochondrial ROS, which were effectively mitigated by NAC (Figs. 3A, B, and S4B), but could not be reduced by deletion of *Zbp1* (Fig. S4H–K). Additionally, in

Fig. 3 DQ induces mitochondrial damage to release Z-DNA and activate ZBP1. A Mitochondrial reactive oxygen species (Mito-ROS) generation in endothelial cells was analyzed by FACS at different time points (0, 4, 6, 8 h) upon DQ stimulation using the MitoSOX probe. **B** Cells treated with DQ for 4 h were subjected to confocal laser scanning microscopy (CLSM) to observe the colocalization of mitochondria and Mito-ROS after staining with Mito-tracker and MitoSOX probes. Nuclei were stained with Hoechst for visualization. Scale bar = 10 μm. **C**, **D** Quantification of total cellular mitochondrial DNA (TC-mtDNA) and cytosolic mitochondrial DNA (Cyto-mtDNA) was performed using qPCR in cells pre-treated with N-Acetylcysteine (NAC, 100 μM) or curcumin (Cur, 10 μM) followed by DQ stimulation. **E** The expression levels of mitochondrial proteins were assessed by western blot analysis at different time points (0, 4, 8, 12, 16 h) post DQ stimulation. **F** Z-DNA formation was detected through immunofluorescence staining using an anti-Z-DNA antibody after DQ stimulation. The specificity of Z-DNA was confirmed by pretreatment with DNase I and RNase A. Nuclei were counterstained with DAPI. Scale bar = 10 μm. **G** Colocalization of Z-DNA and mitochondria was visualized through staining for Tom-20 (mitochondrial marker) and DAPI (nuclei) after DQ stimulation. Mander's overlap coefficients between Z-DNA and Tom-20 were graphed ($n = 10$ for each group), ND not detected. **H** Z-DNA induced by DQ was both sensed and colocalized with ZBP1. Nuclei were stained with DAPI. Scale bar = 10 μm. Mander's overlap coefficients between Z-DNA and ZBP1 were graphed ($n = 10$ for each group), ND not detected.

concordance with the increased ROS levels, there was a concomitant decrease in cellular ATP levels (Fig. S4C). Pretreatment with ROS scavengers, including NAC, GSH, Curcumin, and the glutathione S-transferase P1-1 (GSTP1) inhibitor Ezatiostat, moderately attenuated DQ-induced cell death in ECs (Fig. S4D–G).

Mitochondria constitute a principal source of ROS, thus prompting us to explore downstream signaling following mitochondrial injury. Subsequent investigations focused on mitochondrial DNA (mtDNA). Quantitative PCR analysis of both total cellular and cytosolic mtDNA revealed a decrease in total cellular mtDNA content and an increase in cytosolic mtDNA release from mitochondria. Importantly, both of these effects were ameliorated by pretreatment with NAC and Curcumin (Fig. 3C, D). Western blot analysis of mitochondrial proteins indicated a decrease in BCL2 expression and an increase in BAX expression, underscoring the mitochondrial damage induced by DQ. Notably, DQ treatment resulted in the downregulation of mitochondrial transcription factor A (TFAM), TOP3A, and TOP1MT expression (Fig. 3E). These proteins have previously been reported to play a role in the formation of Z-mtDNA structures [16, 35]. To confirm the occurrence of Z-DNA formation, we performed immunofluorescence staining using a specific anti-Z-DNA antibody. The signaling of Z-DNA significantly increased with DQ treatment, and this signal was abolished by DNase I treatment, but not RNase A, confirming the formation of Z-DNA. Interestingly, Z-DNA signaling was distinct from the nuclei marked by DAPI, suggesting that Z-DNA release did not originate from the nucleus (Fig. 3F). Furthermore, the induced Z-DNA signaling by DQ colocalized with the mitochondrial marker (Tom-20) and ZBP1 (Fig. 3G, H). Collectively, these findings substantiate that DQ-induced mitochondrial damage leads to the release of Z-mtDNA, which is colocalized with ZBP1.

ZBP1 is activated by Z-mtDNA and triggers necroptosis via RIPK3/MLKL

Subsequently, we sought to investigate whether DQ-induced cell death was dependent on ZBP1 in cultured cells. We isolated primary endothelial cells (ECs) from both *WT* and *Zbp1* knockout mice. Upon treatment with DQ, we observed cell death, as evidenced by PI positivity and a decline in cellular ATP levels in *WT* cells. In contrast, the deletion of *Zbp1* effectively blocked DQ-induced cell death (Fig. 4A–C). Notably, it was observed that ZBP1 was not indispensable for DQ-induced mitochondrial damage and ROS production (Fig. S4H–K). These findings collectively indicate that DQ-induced mitochondrial damage leads to the release of mtDNA, subsequently activating ZBP1 to trigger cell death.

To elucidate the molecular mechanism underlying ZBP1-mediated cell death induced by DQ, our investigation honed on the Z-DNA binding domains of ZBP1, specifically Zα1 and Zα2. We devised plasmids with mutated or deleted ZBP1 constructs designed to disrupt the Zα domains (Fig. 4D). Subsequently, reconstitution experiments were conducted using *Zbp1*-deficient cells. The results unequivocally indicated that either the deletion or mutation of Zα1 or Zα2 domains in ZBP1 could not rescue DQ-induced cell death when compared to the *WT* counterparts (Fig. 4E). Additionally, ECs isolated from $Za1a2^{Mut}$ or *Zα1* deletion mice exhibited substantial resistance to DQ-induced cell death in vitro (Fig. S5A, B). In light of ZBP1's possession of RIP homotypic interaction motifs (RHIM) that facilitate interactions with RIPK1/RIPK3, thus triggering necroptosis, we embarked on an exploration of the RHIM's role in DQ-induced cell death. Notably, deletion of the RHIM domain (ΔRHIM) within ZBP1 could not rescue DQ-induced cell death (Fig. 4E).

Subsequently, we subjected to analyze ZBP1-containing complex. Upon DQ treatment, ZBP1/RIPK3/MLKL assembled into a functional complex, that was regulated by both the Zα and RHIM domains of ZBP1 (Fig. 4F). The physical interactions between ZBP1 and RIPK3 induced by DQ were further confirmed in the proximity ligation assay (PLA) (Fig. 4G, H). Importantly, the mutation of either the Z-DNA sensing domain, Zα, or pretreatment with DNase I disrupted the ZBP1/RIPK3 complex (Fig. 4F–H), strongly suggesting that Z-mtDNA likely serves as the initiator of this signaling cascade. Specifically, ZBP1, activated by Z-mtDNA, recruits RIPK3 via the RHIM domain in response to DQ stimulation (Fig. 4F).

To further affirm the critical role of Z-DNA sensing domain in vivo, we generated mice with mutations in *Zα* ($Za1a2^{Mut}$) and mice with *Zα1* deletion *(ΔZα1)*. Both the $Za1a2^{Mut}$ and *ΔZα1* mice demonstrated noteworthy multiorgan protection following DQ treatment (Figs. 4I–N, and S5C–J). Western blot analysis unveiled a substantial increase in the phosphorylation of RIPK3 and MLKL, a phenomenon significantly mitigated by either *Zbp1* deletion or $Za1a2^{Mut}$ (Fig. 4O) in ECs. These findings led us to posit that RIPK3 may function as the downstream signaling molecule responsible for initiating cell death in response to DQ stimulation.

RIPK3/MLKL dependent necroptosis partially contributes to DQ-induced organ damage

Building upon the insights presented in Fig. 1, which illustrated the partial protection afforded by *Mlkl* knockout mice against DQ-induced organ injury, our subsequent aim was to scrutinize the distinct roles played by RIPK3 and MLKL in DQ-induced cell death. Remarkably, the deletion of *Zbp1* or *Ripk3* significantly thwarted DQ-induced cell death, whereas *Mlkl* deficiency only moderately attenuated this mode of cell demise in isolated ECs (Figs. 5A, B and S6A–I). Mutation of RHIM and kinase activity of RIPK3 could not rescue DQ-induced cell death (Figs. 5C, D and S7G). However, either deletion of *Ripk3* or *Mlkl* completely blocked necroptosis induced by TNFα in combination with the IAP inhibitor (LCL161) and ZVAD (TLZ) in ECs (Fig. S7A, B). These data suggest the existence of another mechanism downstream of the ZBP1/RIPK3 axis that potentially contributes to DQ-induced cell death. Similar trends were observed in $Ripk3^{-/-}$ renal tubular epithelial cells (TECs) and even mouse fibrosarcoma L929 cells. Intriguingly, the absence of *Ripk3* not only hindered cell death triggered by DQ but also completely abrogated necroptosis elicited by other stimuli such as TLZ in TECs or TZ for L929 cells

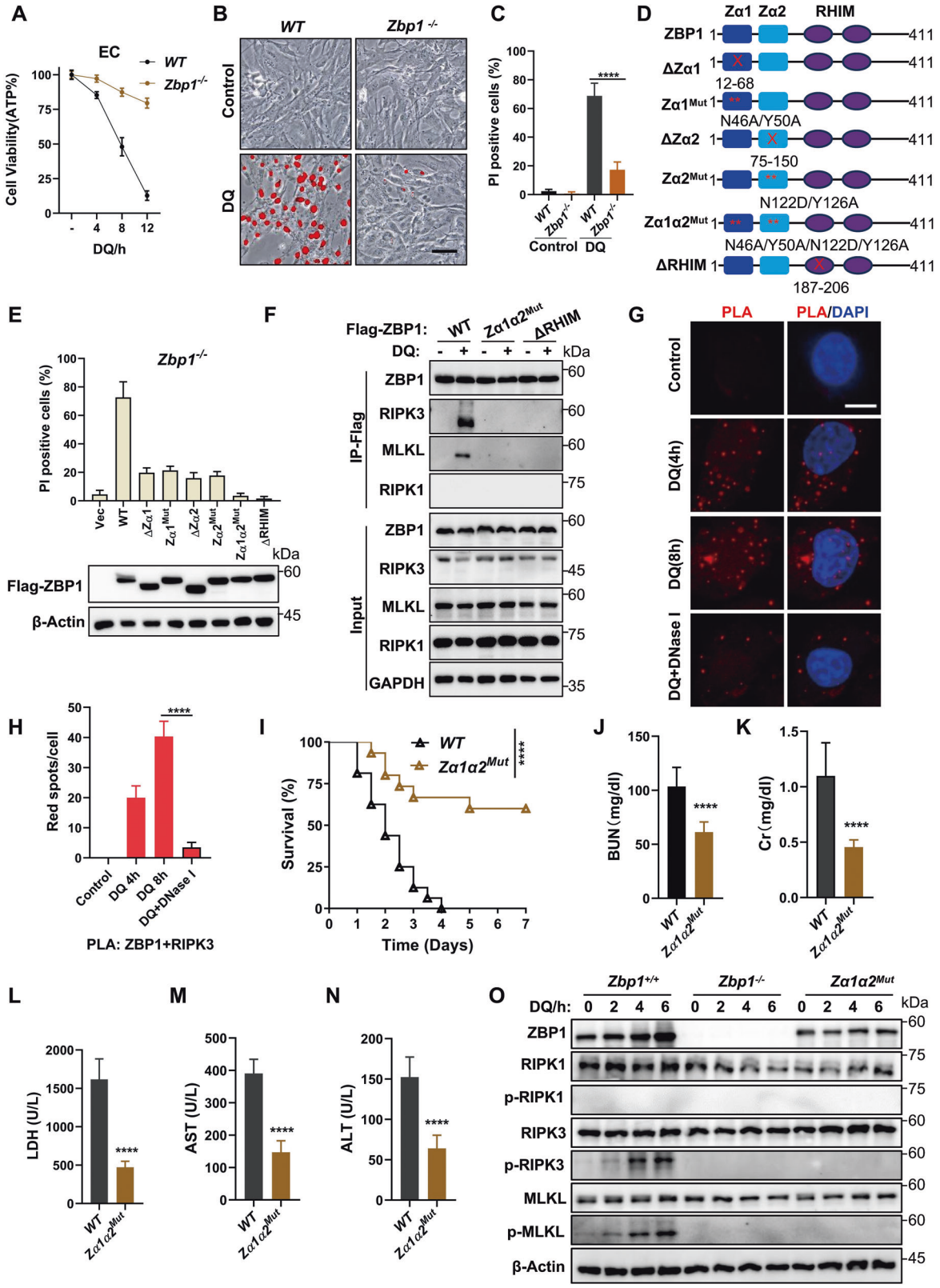

(Fig. S7C–I). Along similar lines in ECs, *Mlkl* deficiency only moderately attenuated DQ-induced cell death, but completely abrogated necroptosis induced by TZ in L929 cells (Fig. S7H). Of note, ferroptosis induced by RSL3 remained unaffected by the absence of RIPK3, thus affirming the dispensable role of RIPK3 in the canonical ferroptosis pathway (Fig. S7J). Consistent with the in vivo evidence, where pretreatment with ZVAD or Nec-1 failed to confer protection against DQ-induced lethality in mice (Fig. S1A), neither the deletion of *Caspase-8* (*Casp8*) or *Ripk1* nor treatment with ZVAD or Nec-1 had any discernible effect on DQ-induced cell

Fig. 4 The Zα and RHIM domain facilitates the activation of ZBP1 and its interaction with RIPK3 to trigger cell death in response to DQ stimulation. **A** Viability of primary endothelial cells (ECs) isolated from *Zbp1* knockout (*Zbp1*$^{-/-}$) mice and *wild-type* (*WT*) mice after DQ treatment. **B** Representative PI staining images showing EC cell death induced by DQ. ECs were isolated from *WT* and *Zbp1*$^{-/-}$ mice. Scale bar = 200 μm. **C** Quantification of cell death for (**B**) using PI/Hoechst staining and Image J software. **D** Diagram illustrating the structure of ZBP1 and the strategy of mutation and deletion. **E** *Zbp1*$^{-/-}$ ECs were infected with lentivirus carrying vector variants encoding Flag-ZBP1-WT, ΔZα1, Zα1^{Mut}, ΔZα2, Zα2^{Mut}, Zα1α2^{Mut}, or ΔRHIM. DQ-induced cell death was evaluated using PI/Hoechst staining. Western blot analysis was conducted using anti-Flag antibody, and β-actin served as a loading control. **F** ZBP1/RIPK3/MLKL necrosome formation initiated by the RHIM and Zα domain of ZBP1 was immunoprecipitated using anti-Flag M2 beads in *Zbp1*$^{-/-}$ ECs reconstituted with Flag-ZBP1-WT, Zα1α2^{Mut}, or ΔRHIM. **G** Proximity ligation assay (PLA) examining the physical interaction between ZBP1 and RIPK3 in WT ECs at 4 and 8 h after DQ treatment, DNase I was added to digested DNA. Red spots indicate positive PLA signals. Nuclei were counterstained with DAPI. Scale bar = 10 μm. **H** Quantification of PLA signals from (**G**). **I**–**N** the mice were subjected to DQ treatment as described in Fig. 1. **I** Survival rate ($n = 15$) monitored over time. Blood samples ($n = 7$) analyzed for BUN (**J**), Cr (**K**), LDH (**L**), AST (**M**), and ALT (**N**) through ELISA ($n = 6$). ****$P < 0.0001$. **O** Western blot analysis of phosphorylated RIPK1/RIPK3/MLKL, total RIPK1/RIPK3/MLKL/ZBP1 in ECs isolated from mice of various genotypes at different time points after DQ treatment.

death in L929 cells (Figs. 5C, and S7H, I). Collectively, these findings signify that under DQ stimulation, ZBP1/RIPK3/MLKL assemble into a physical complex that executes necroptosis independently of RIPK1 kinase activity and Casp8.

ZBP1/RIPK3 axis triggers ferroptosis contributing to DQ-induced organ failure

To explore the downstream signaling pathways initiated by ZBP1/RIPK3, independent of MLKL, we conducted a series of additional experiments. Both scRNA-seq and western blot data conclusively indicated a significant involvement of the NRF2/HO-1 pathway in response to DQ stimulation (Figs. 1O, 2B, 5E). Furthermore, our investigations revealed a substantial increase in lipid-ROS levels under DQ treatment. Notably, the deletion of either *Zbp1* or *Ripk3* entirely abrogated the production of lipid-ROS, whereas the deficiency of *Mlkl* had no discernible impact on this process (Fig. 5F and Fig. S6J). Additionally, the application of two lipid-ROS scavengers, ferrostatin-1 (Fer-1) and liproxstatin-1 (Lip-1), not only quelled lipid-ROS production but also markedly suppressed DQ-induced cell death (Fig. 5G, H). In summary, these findings collectively imply that DQ treatment elicits ferroptosis downstream of the ZBP1/RIPK3 axis in vitro.

The presented data thus revealed the existence of two distinct cell death pathways initiated by DQ stimulation: MLKL-mediated necroptosis and ferroptosis. When we compared the effects of Lip-1 treatment alone with *Mlkl* deletion, it was strikingly evident that pretreatment with Lip-1 in *Mlkl* knockout ECs comprehensively obstructed DQ-induced necroptosis and ferroptosis (Fig. 5I, J). Importantly, the strategic combination of negating necroptosis via *Mlkl* gene deletion and inhibiting ferroptosis through the utilization of the lipid-ROS scavenger Lip-1 yielded remarkable protection against DQ-induced organ failure in mice, ultimately culminating in a notable enhancement in survival rates (Figs. 5K–O and S8A–D). This synergistic approach effectively prevented cell death, thereby highlighting its potential as a promising therapeutic strategy for the amelioration of DQ-induced fatal organ injury.

RIPK3 phosphorylated FSP1 to trigger ferroptosis via inhibition of FSP1's NADH-dependent oxidoreductase activity

Given GPX4 is important for scavenge phospholipid peroxides to prevent ferroptosis, we further detected the expression of GPX4. The protein level of GPX4 decreased in the lung, liver and kidney tissue of *WT* mice when exposed to DQ. However, deletion of *Zbp1* or *Ripk3* or *Mlkl* did not inhibit the decrease of GPX4 (Figs. 1O, 5E and S1C, D). In our pursuit to unveil additional constituents of the ZBP1/RIPK3 pathway that play a role in ferroptosis, we meticulously analyzed the RIPK3 interactome data as previous reported [36]. Within this dataset, we unearthed ferroptosis suppressor protein 1 (FSP1), also recognized as apoptosis-inducing factor mitochondrial 2 (AIFM2), as a robust partner of RIPK3, particularly within the context of cell death (Fig. S9A). Since single-cell RNA sequencing (Figs. 2B and S3L) and western blotting (Fig. 1O, Fig. S1C, Fig. S1D, Fig. 5E) showed that DQ did not significant affect the expression of FSP1, we validated the interaction between RIPK3 and FSP1 through co-immunoprecipitation (Co-IP) assays conducted in HEK293T cells (Fig. 6A). The pull-down of His-RIPK3 occurred alongside His-FSP1 that was coupled with protein A/G beads by anti-FSP1 antibody, further affirming the direct interaction between FSP1 and RIPK3 (Fig. 6B). Crucially, we ascertained that DQ induced the formation of a functional complex encompassing ZBP1/RIPK3/MLKL/FSP1, which was nucleated through the RHIM interaction between RIPK3 and ZBP1 (Fig. 6C). Furthermore, the physical interaction between FSP1 and RIPK3 was reinforced through proximity ligation assays and immunofluorescence staining conducted under DQ stimulation (Figs. 6D, E and S9B).

We then proceeded to investigate the involvement of FSP1 in DQ-induced ferroptosis. Notably, the ectopic expression of FSP1-Flag exerted a pronounced inhibitory effect on DQ-induced cell death in ECs in a dose-dependent manner (Fig. 6F). In contrast, knockout of *Fsp1* rendered the cells notably more susceptible to DQ-induced cell death in L929 cells (Figs. 6G and S9C). Of note, L929 cells with *Fsp1* deficiency did not display more susceptible to cell death induced by TNFα plus ZVAD, indicating that FSP1 is dispensable for canonical necroptosis (Fig. S9D). In an in vivo context, the targeted deletion of endothelial *Fsp1* yielded a significant increase in mouse mortality (Fig. S9E). Collectively, these results unequivocally affirm the pivotal protective role played by FSP1 in mitigating DQ-induced cell death and subsequent organ injury.

FSP1 is well-established as an NAD(P)H-dependent coenzyme Q_{10} (CoQ_{10}) oxidoreductase, where the reduced CoQ_{10} functions as a radical-trapping antioxidant, effectively suppressing lipid peroxidation and ferroptosis [23, 24]. Consequently, we embarked on an investigation to ascertain whether RIPK3 could hinder the oxidoreductase activity of FSP1. As depicted in Fig. 6H, in the presence of RIPK3, but not kinase-dead form of RIPK3 (KD, D161N), the NADH consumption associated with FSP1-mediated reduction of CoQ_{10} was markedly impaired. This observation unequivocally indicates that the interaction between RIPK3 and FSP1 resulted in the suppression of FSP1's oxidoreductase activity.

Given the pivotal role of RIPK3 kinase activity in DQ-induced cell death (Fig. 5D) and FSP1's oxidoreductase inhibition (Fig. 6H) and the established interaction between RIPK3 and FSP1 (Fig. 6B, C), we posited that RIPK3 may impede the oxidoreductase activity of FSP1 through phosphorylation. Indeed, following DQ stimulation, we observed the phosphorylation of FSP1, as detected through phospho-tag SDS-PAGE. The phospho-band of FSP1-Flag was discerned in FSP1-Flag ectopic expression WT ECs, affirming DQ-dependent phosphorylation of FSP1 (Fig. S10A). To identified the phosphorylation sites, FSP1-Flag was cotransfected with HA-RIPK3, then the immunoprecipitated proteins were subjected to mass spectrometry analysis (MS/MS), five phosphopeptides,

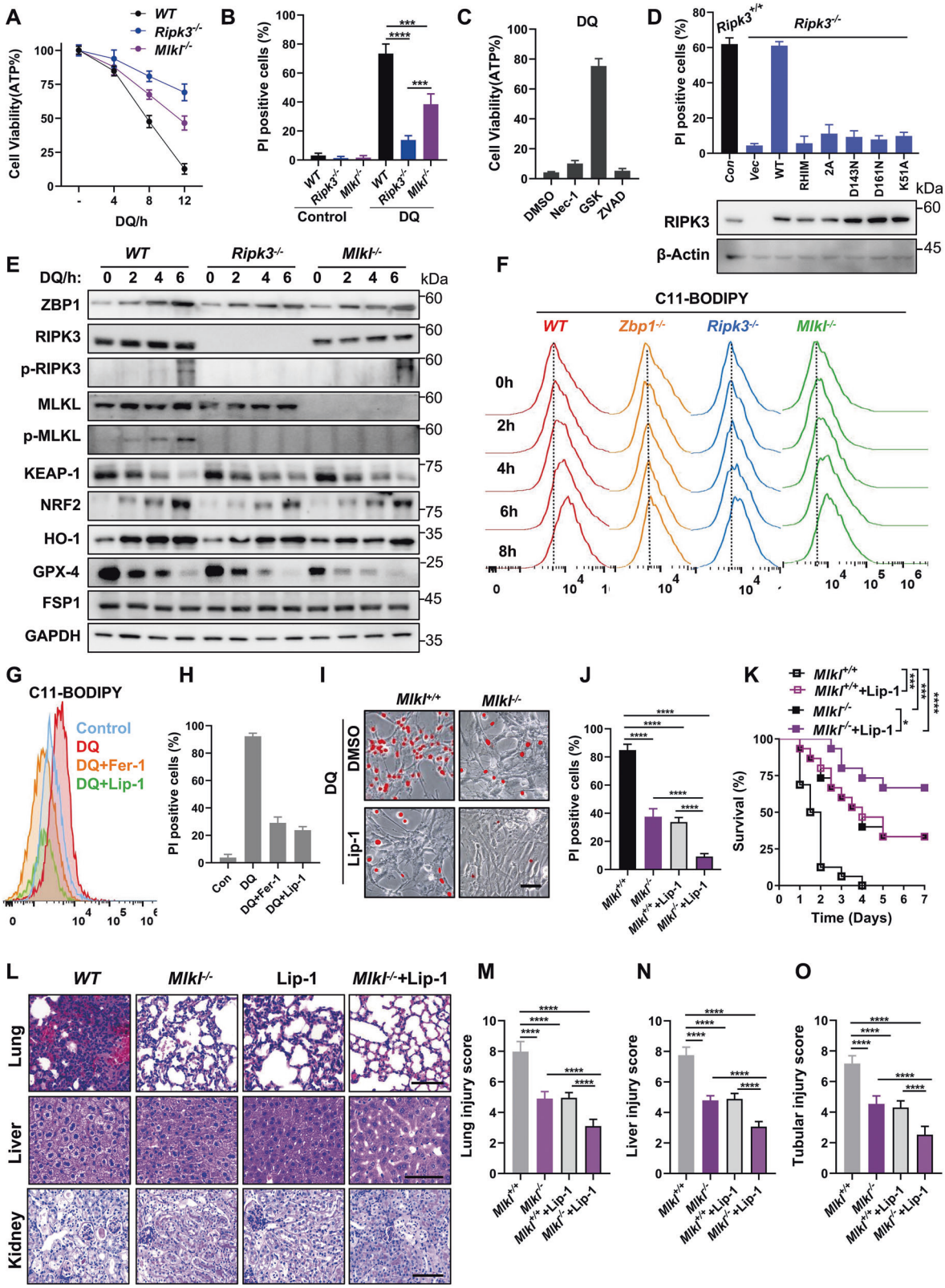

encompassing four conserved phosphorylation sites (T163, T171, S210, S362) on FSP1 were identified (Fig. S10B–D). To probe the functional significance of these phosphorylation sites, we engineered phosphomimic mutants for each site and introduced them into *Fsp1*-KO L929 cells. Our results unveiled that, akin to FSP1-WT, the T171E, S210E, and S362E mutants exhibited anti-DQ-induced cell death effects. However, the T163E mutant failed to suppress cell death induced by DQ (Fig. 6I). Notably, the oxidoreductase activity of HEK293T immunoprecipitated FSP1 T163E mutant was significantly diminished when compared to the inhibitory effect of

Fig. 5 ZBP1/RIPK3 mediates necroptosis and ferroptosis induced by DQ. A Time series illustrating the cell viability detected after DQ treatment. ECs were isolated from *WT*, *Ripk3*$^{-/-}$, and *Mlkl*$^{-/-}$ mice. **B** Quantification of DQ-induced cell death in ECs from *WT*, *Ripk3*$^{-/-}$, and *Mlkl*$^{-/-}$ mice using PI/Hoechst staining and Image J software. **C** Cell viability after pretreatment with RIPK1 inhibitor (Necrostain-1/Nec-1), RIPK3 inhibitor (GSK-843/GSK), pan-caspase inhibitor (ZVAD), or DMSO followed by DQ stimulation. **D** *Ripk3*$^{-/-}$ ECs were transduced with lentivirus containing Flag-RIPK3-WT, RHIM-mutant (Q449A/I450A/G451A), T231A/S232A (2A), D143N, D161N, K51A constructs. DQ-induced cell death was quantified using PI/Hoechst staining and probed with anti-RIPK3 antibody by western blot analysis. β-actin served as a loading control. **E** Western blot analysis of ZBP1, necroptotic, and antioxidant proteins in ECs isolated from mice of different genotypes after DQ treatment. **F** Detection of DQ-induced lipid ROS using C11-bodipy probe by FACS at various time points in *WT*, *Zbp1*$^{-/-}$, *Ripk3*$^{-/-}$, *Mlkl*$^{-/-}$ ECs. **G** Pretreatment with Ferrostatin-1 (Fer-1) or liproxstatin-1 (Lip-1) followed by DQ stimulation in *WT* ECs. Lipid ROS levels were measured using C11-bodipy probe by FACS. **H** Measurement of cell death after pretreatment with Fer-1 or Lip-1 followed by DQ stimulation, quantified using PI/Hoechst staining. **I** Representative images of PI staining showing DQ-induced EC cell death in *WT* and *Mlkl*$^{-/-}$ ECs with or without Lip-1 pretreatment. Scale bar = 200 μm. **J** Quantification of DQ-induced cell death as PI-positive cells in six randomly selected fields from (**I**). **K**–**O** the mice were subjected to DQ treatment as described in Fig. 1. **K** Survival rates ($n = 15$) monitored over time in *Mlkl*$^{-/-}$ and *WT* control mice with or without 10 mg/kg Lip-1 pretreatment 24 h and 1 h before DQ treatment. **L**–**O** Histologic lung, liver, and renal injury scores in the indicated mice. Scoring was performed in at least 10 randomly selected fields per mouse. $n = 6$. *$P < 0.05$, **$P < 0.01$, ***$P < 0.001$.

RIPK3 on FSP1-WT (Fig. 6J). To further corroborate these findings, we purified recombinant FSP-WT and T163E from *E. coli* (Fig. 6K) and conducted an in vitro oxidoreductase assay. Remarkably, rFSP1-T163E almost entirely lost its oxidoreductase activity (Fig. 6L, M), thereby confirming the indispensable role of T163 phosphorylation in suppressing FSP1 activity. Furthermore, we explored the cellular localization of FSP1-WT and T163E. Under DQ stimulation, akin to FSP1-WT-GFP that interacts with RIPK3 and forms puncta, FSP1-T163E-GFP independently condenses into puncta (Figs. S9B and S10E). Collectively, our findings reveal that upon DQ stimulation, RIPK3 engages in an interaction with and phosphorylates FSP1, thereby inhibiting its oxidoreductase activity and consequently contributing to ferroptosis.

Vitamin K recovers DQ-induced ferroptosis in vitro and organ failure in vivo through restoring the oxidoreductase activity of FSP1

A recent investigation has elucidated that vitamin K (VK) can be effectively reduced to its hydroquinone form by FSP1, a potent radical-trapping antioxidant known for its cellular protection against ferroptosis [26]. Armed with this knowledge, our study delved into the potential of VK to rescue DQ-induced ferroptosis. Initially, we explored the NADH-dependent oxidoreductase activity of FSP1 using VK as a substrate. Analogous to CoQ_{10}, FSP1 efficiently reduced VK, concomitant with NADH consumption. Notably, this reduction process was subject to inhibition by RIPK3 (Fig. 7A). Subsequently, VK1, VK2, and VK3 not only demonstrated substantial reductions in lipid ROS production (Fig. 7B), but also exhibited concentration-dependent inhibition of DQ-induced ferroptosis in ECs (Fig. 7C–E). We then turned attention to the in vivo role of VK in counteracting DQ-induced organ failure. As depicted in Fig. 7F–J, MK4, a form of VK2, significantly enhanced mice survival and mitigated lung, liver, and kidney injuries. TUNEL staining underscored that MK4 effectively reduced cell death in DQ-treated lung, liver, and kidney tissues (Fig. 7K–N). Remarkably, the concurrent prevention of necroptosis through *Mlkl* gene deletion and the suppression of ferroptosis via vitamin K supplementation bestowed robust protection against DQ-induced organ failure in mice (Fig. S11B–E). This dual strategy ultimately translated to a marked enhancement in the survival rate (Fig. S11A).

DISCUSSION

In this study, we have uncovered the crucial role of Z-mtDNA within endothelial cells as a novel signaling molecule in response to oxidative stress provoked by DQ poisoning. Additionally, we have revealed the pivotal role of ZBP1 in orchestrating the pathological ramifications stemming from DQ exposure, encompassing both the RIPK3-dependent necroptotic and ferroptotic pathways. Our investigation has unmasked that the Zα domain within ZBP1 is indispensable for its activation in the context of DQ-induced Z-mtDNA formation. Concurrently, the RHIM domain of ZBP1 triggers the activation of RIPK3, which subsequently leads to the phosphorylation of both MLKL and FSP1. This intricate chain of events ultimately culminates in the execution of necroptosis and ferroptosis. Furthermore, scRNA-seq data indicate that endothelial cells suffer severe damage, with a drastic reduction in cell numbers at the early stage exposure to DQ. Notably, the deletion of *Zbp1* and *Ripk3* specifically in endothelial cells, rather than bone marrow-derived cells, confers protection against the lethal organ damage induced by DQ. These findings strongly suggest that endothelial cell death plays a pivotal role in the development of DQ-induced multiple organ damage.

Excessive oxidative stress within the mitochondria emerges as a central mechanism that underlies DQ-induced cell death. Previous research has already established that the introduction of ROS scavengers effectively curtails the generation of mtDNA and subsequently prevents cellular demise. This process involves a decline in the levels of TFAM and TOP3A, contributing to instability within the mitochondrial genome and facilitating the release of Z-mtDNA [7, 37]. Notably, our study reveals that DNase I has the capacity to effectively block the formation of Z-mtDNA, thereby disrupting the interaction between ZBP1 and RIPK3. Furthermore, the introduction of mutations within the Zα domain of ZBP1 appears to impede its activation and its interaction with RIPK3, resulting in the inhibition of RIPK3 phosphorylation and, subsequently, the prevention of cell death. These findings underscore the critical role played by the accumulation of Z-mtDNA in initiating the activation of ZBP1 upon DQ stimulation.

ZBP1 is widely acknowledged for its distinctive capability to engage in homotypic interactions with RHIM -containing proteins such as RIPK1 and RIPK3. These interactions lead to the activation of RIPK3 and its downstream effector, MLKL, ultimately driving necroptosis. Recent studies have postulated that ZBP1, particularly through its Zα domain, might act as a specific trigger for PANoptosis, which encompasses a range of programmed cell death modalities including apoptosis, necroptosis, and pyroptosis, in response to influenza A virus (IAV) infection [38]. Our current investigation provides novel insights into the role of ZBP1 following DQ poisoning. We observe that, upon DQ stimulation, ZBP1 forms a complex containing RIPK3, MLKL, and FSP1, indicating a potential role for ZBP1 as a specific upstream trigger for both necroptosis and ferroptosis. Interestingly, we find that the deletion of either *Zbp1* or *Ripk3* robustly attenuates cell death. However, the loss of *Mlkl* or the pharmacological inhibition of ferroptosis alone does not completely rescue cell death. Combining the deletion of *Mlkl* with VK or other ferroptosis inhibitor treatment proves highly effective in mitigating multiorgan damage and lethality caused by DQ. These findings strongly demonstrated both necroptosis and ferroptosis contributed to DQ-induced fatal organ injury.

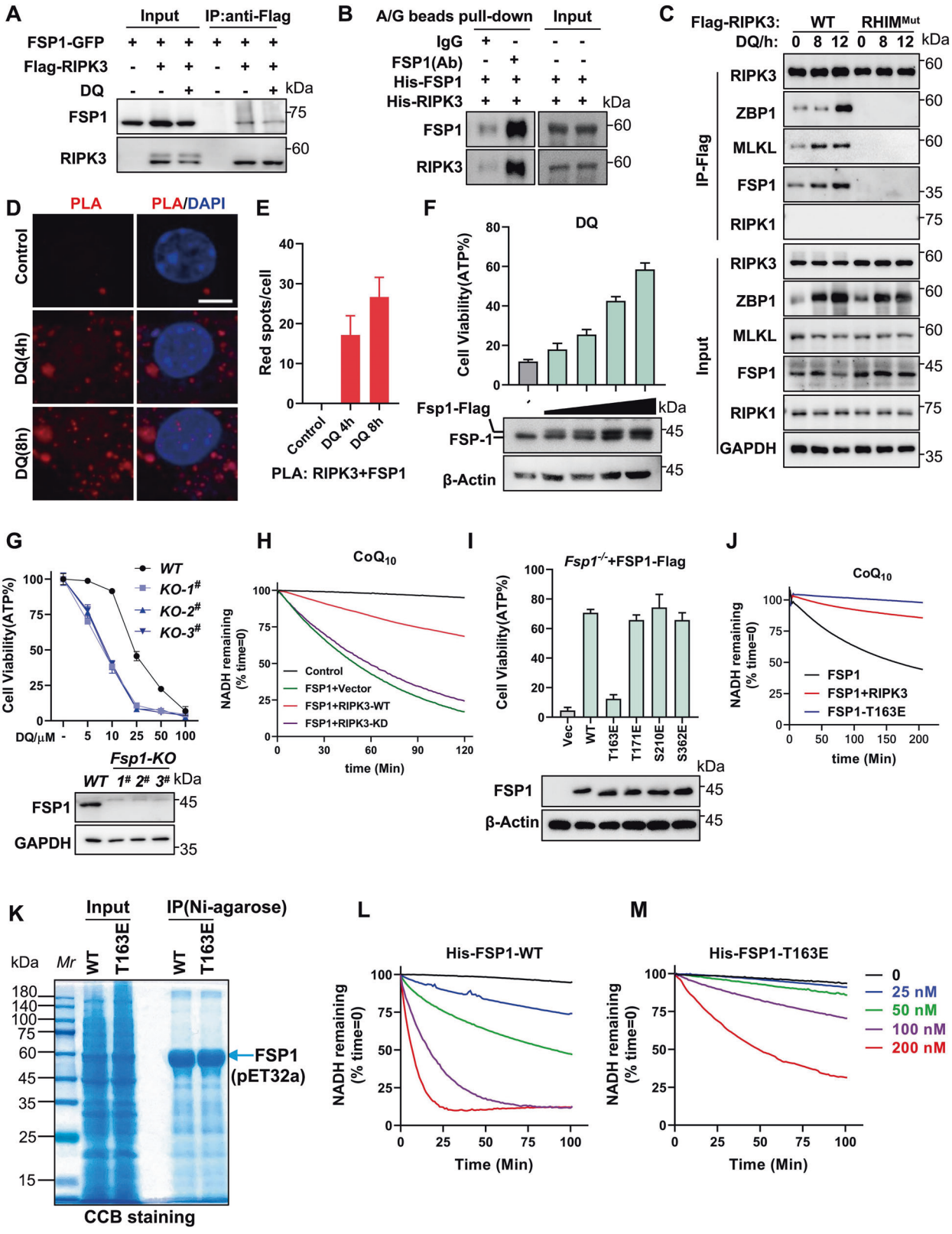

Prior research has suggested that the plasma membrane localization of FSP1 is pivotal in preventing ferroptosis, which acts parallel to GPX4 to inhibit ferroptosis [23, 24]. Nonetheless, a recent study by Conrad *et al.* has identified a novel inhibitor, icFSP1 (3-phenylquinazolinones), which targets FSP1. This compound induces the subcellular relocalization of FSP1 from the membrane, promotes phase condensation, and ultimately triggers ferroptosis [39]. Interestingly, DQ did not significantly affect the expression of FSP1. However, our investigation further reveals that RIPK3 recruits FSP1 to form a cytosolic death complex. This complex phosphorylates FSP1,

Fig. 6 DQ-triggered ferroptosis is mediated through the RIPK3/FSP1 axis. A Co-immunoprecipitation confirmed the interaction between RIPK3 and FSP1. HEK293T cells were cotransfected with FSP1-GFP and Flag-RIPK3, followed by immunoprecipitation of Flag-RIPK3 with anti-Flag M2 beads. **B** The recombinant mouse-derived RIPK3 protein, expressed by *P. pastoris*, with N-6*His labeled tag, His-FPS1 purified from *E. coli* was coupled with protein A/G beads and anti-FSP1 antibody, then pull-down assay was performed. **C** The ZBP1/RIPK3/MLKL/FSP1 death complex induced by DQ was detected by immunoprecipitation using anti-Flag M2 beads from Flag-RIPK3 (WT, $RHIM^{Mut}$) reconstituted $Ripk3^{-/-}$ ECs under DQ stimulation. **D** Detection of physical associations between FSP1 and RIPK3 through proximity ligation assay (PLA) in *WT* ECs after DQ treatment for 4 and 8 h. Red spots indicate interactions. Scale bar = 10 μm. **E** Quantification of PLA signaling for (**D**). **F** Expression-dependent resistance to DQ-induced cell death by ectopic expression of FSP1-Flag in *WT* ECs. Western blot analysis was performed using anti-FSP1 antibody, and β-actin served as loading control. **G** Sensitivity of *Fsp1*-knockout L929 cells to DQ-induced cell death. Different concentrations of DQ were applied to *Fsp1*-knockout and *WT* L929 cells, and cell viability assayed. Western blot analysis confirmed FSP1 deficiency in *Fsp1*-knockout cells, with β-actin as loading control. **H** Measurement of NADH-dependent oxidoreductase activity of FSP1 alone or with RIPK3 (WT; KD, kinase dead, D161N) using CoQ_{10} as substrate. Co-transfection of FSP1-Flag and HA-RIPK3 or vector, then FSP1 was immunoprecipitated using anti-Flag M2 beads. NADH-dependent oxidoreductase activity assay was carried out as described in the Methods section. **I** DQ-induced cell death detected by cell viability assay in $Fsp1^{-/-}$ L929 cells infected with lentivirus containing FSP1-Flag-WT, T163E, T171E, S210E, S362E constructs. **J** Measurement of NADH-dependent oxidoreductase activity in the FSP1-Flag immunoprecipitants of HEK293T cells cotransfected with FSP1-WT or T163E and RIPK3 for 36 h. **K** Coomassie brilliant blue staining of recombined FSP1 (rFSP1-WT, T163E) purified from *E. coli*. **L**, **M** Measurement of NADH-dependent oxidoreductase activity of recombined FSP1 (rFSP1-WT, T163E).

inhibiting its NAD(P)H-ubiquinone reductase function and sequestering FSP1 in the cytosol. This process culminates in condensation with RIPK3, ultimately triggering ferroptosis. Importantly, the absence of FSP1 exacerbates DQ-induced cell death and organ injury. However, sustaining FSP1 activity through the supply of vitamin K partially mitigates DQ-induced cell death and subsequent organ damage. Notably, we demonstrated T163 is a key site for FSP1 phosphorylation by RIPK3, and further revealed the indispensable role of T163 phosphorylation in suppressing FSP1 activity.

In summary, our study highlights the significance of Z-mtDNA-mediated ZBP1/RIPK3-dependent necroptosis and ferroptosis in endothelial cells as key contributors to the development of organ failure induced by DQ poisoning (Fig. 8). Furthermore, our findings suggest that a comprehensive intervention strategy targeting both necroptosis and ferroptosis holds promise as an effective approach to mitigate the deleterious effects of DQ-induced organ damage.

MATERIALS AND METHODS

Mice

All the mice used in this study are C56BL/6J background. $Zbp1^{-/-}$, $Ripk3^{-/-}$, $Mlkl^{-/-}$ and $Gsdmd^{-/-}$ mouse strains were gifts from Dr. Jiahuai Han at the School of Life Sciences, Xiamen University, China [40–42]. *Zbp1-Za1a2*^{Mut} mice were kindly supplied by Prof. Wei Mo at Xiamen University, China [43]. *Zbp1-ΔZa1* mice with a deletion of 168 bp in exon2 of *Zbp1* genome (24th amino acid-69th amino acid deletion of ZBP1) were kindly gift from Prof. Ben Lu at Central South University, China. $Mlkl^{fl/f}$, $Zbp1^{fl/fl}$ and $Fsp1^{fl/fl}$ mice were obtain from GemPharmatech, Nanjing, China. We acquired *Tie2-Cre*, *Vav-iCre* and $Ripk3^{fl/fl}$ mice from Jackson Laboratory. Male mice (10- to 12-week-old, 24–28 g body weight) were used in this study. A detailed description of their genetic background and how KO strains were generated were provided in Supplementary information.

Single-cell transcriptome sequencing

Sample source and methodologies are detailed in the Supplementary data description of "Materials and methods".

Western blot analysis, co-immunoprecipitation assay and antibodies

Detailed methods and antibodies were provided in Supplementary information.

Mitochondrial DNA isolation and quantitative PCR

For the cytosolic fractionation and subsequent DNA isolation process, we adopted a protocol as previously outlined [44]. Detailed methods were provided in Supplementary information.

Cell culture

Mouse renal tubular epithelial cells TCMK-1 (TECs) were obtained from ATCC (CCL-139™); HEK293T cells and mouse fibrosarcoma L929 cell lines, encompassing *Zbp1-KO, Ripk1-KO, Ripk3-KO, Mlkl-KO*, and *Casp8-KO* cells, were generously provided by Prof. Jiahuai Han from the School of Life Sciences, Xiamen University, China. These cells were cultured in Dulbecco's Modified Eagle's Medium (DMEM) supplemented with 10% fetal bovine serum (FBS), 4 mM L-glutamine, 100 IU penicillin, and 100 mg/mL streptomycin, and maintained at 37 °C in a humidified incubator with 5% CO_2.

Proximal tubules were freshly isolated as previously described in our study [45]. After approximately 4–5 days of cultivation, primary proximal tubular cells (PTCs) were employed in subsequent experiments.

Mouse lung microvascular endothelial cells (ECs) were prepared as detailed in a previous publication [46]. Detailed methods were provided in Supplementary information.

Generation of knockout cell lines using the CRISPR-Cas9 technique

The knockout of *Ripk3* and *Fsp1* in mouse cell lines was achieved through the utilization of the CRISPR-Cas9 system. The targeted sequences for gRNA were as follows: 5′-gtgggacttcgtgtccgggc-3′ for mouse *Ripk3* and 5′-tgcacgtggtgatcgtgggc-3′ for mouse *Fsp1*. Detailed methods were provided in Supplementary information.

Cell viability and cell death assessment

The assessment of cell viability was conducted employing the Cell Titer-Glo Luminescent Cell Viability Assay Kit (Promega, G7571). For cell death assessment, cells were exposed to a staining solution containing 1 μg/ml propidium iodide (PI) and 2 μg/ml Hoechst-33342 for 10 min at 37 °C. Detailed methods were provided in Supplementary information.

Plasmid construction

pBOBI-N-Flag-ZBP1 and pBOBI-N-Flag-ZBP1-mutations ($Zα2^{Mut}$, ΔRHIM) were generously provided by Prof. Ben Lu from Central South University. Additionally, pBOBI-N-Flag-RIPK3 was provided by Prof. Jiahuai Han at Xiamen University. The detail construction was provided in Supplementary information.

Mass spectrometry analysis

FSP1-Flag was cotransfected with HA-RIPK3 or vector in HEK293T cells, then immunoprecipitated using Anti-DYKDDDDK-Tag mAb agarose conjugated beads (Abmart, M20018), then eluted twice with 0.15 mg/ml of 3X Flag peptide with N-terminal biotin tag in HBS lysis buffer for 30 min each time, and the elution was pooled for a final volume of 300 μl. The details of MS experiments were provided in Supplementary information.

Protein purification and activity assays

Flag-tagged wild-type (WT) FSP-1 and its mutants were cotransfected with either RIPK3 or an empty vector, then FSP1-Flag was immunoprecipitated.

The recombinant FSP1 proteins, including wild-type (FSP1-WT) and the T163E mutant were expressed in *Escherichia coli* BL21(DE3) and induced with 1 mM isopropyl β-D-1-thiogalactopyranoside (IPTG) overnight at 20 °C. Purification of the recombinant proteins was achieved using BeyoGold™ His-tag Purification Resin (sourced from Beyotime, P2226).

For the assessment of NADH oxidation kinetics, FSP1-Flag immunoprecipitants or recombinant FSP1 were incubated with 500 μM NADH and

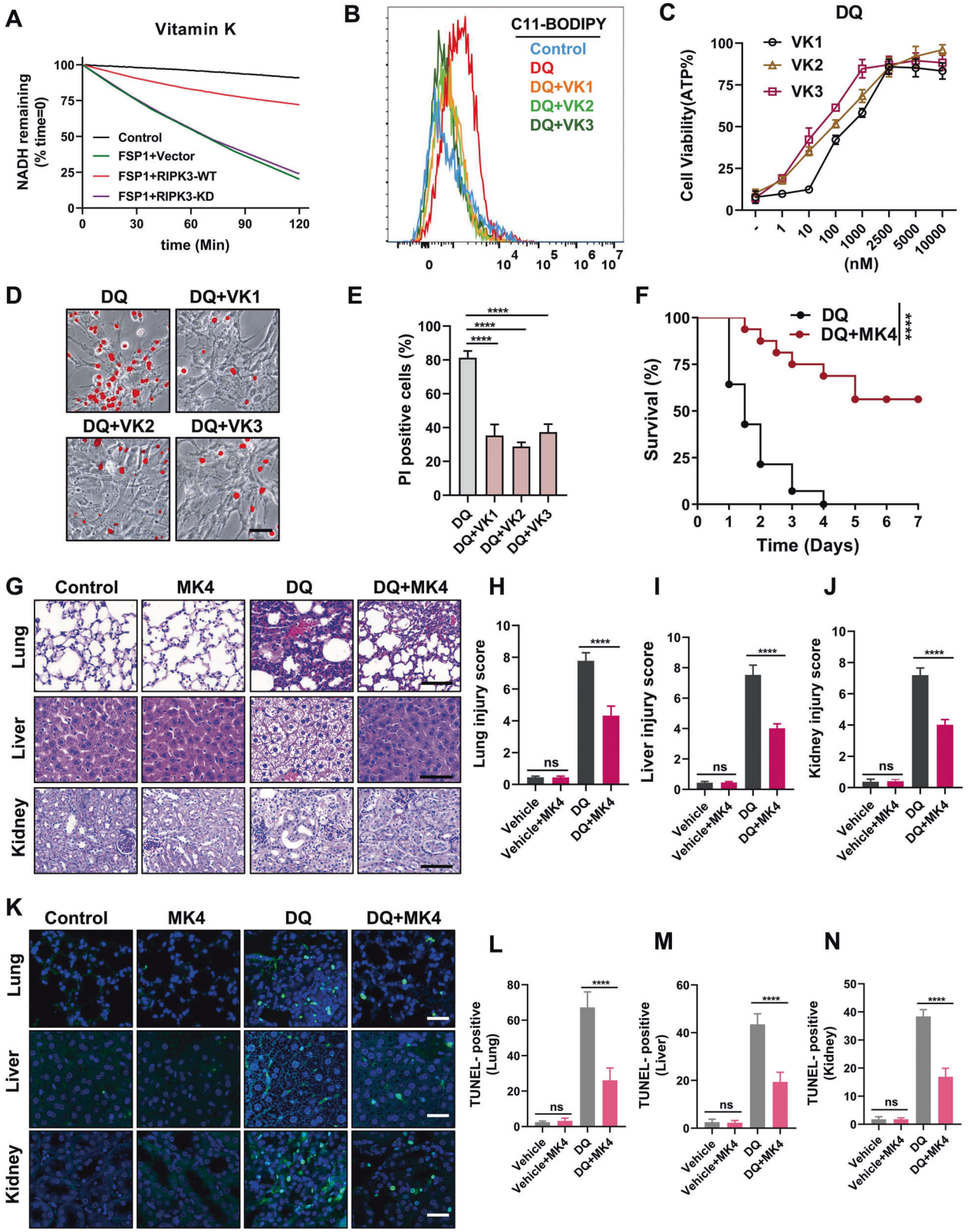

500 μM coenzyme Q_{10} or Vitamin K in a total volume of 100 μl PBS. The reduction in absorbance at 340 nm, indicative of NADH oxidation, was monitored over a 100-minute time frame. Detailed methods were provided in Supplementary information.

Duolink proximity ligation assay

Proximity ligation assays were conducted employing the Duolink system (obtained from Sigma-Aldrich). Detailed methods were provided in Supplementary information.

Fig. 7 Vitamin K counteracts DQ induced cell death both in vitro and in vivo through restoring FSP1 activity. A The NADH-dependent oxidoreductase activity of FSP1, either alone or in combination with RIPK3 (WT, or kinase-dead, D161N), was measured using Vitamin K as a substrate. The NADH-dependent oxidoreductase assay was conducted as described in the Methods section. **B** Vitamin K1/K2/K3 inhibited the production of lipid ROS induced by DQ. After WT ECs were pre-treated with Vitamin K1/K2/K3 and stimulated with DQ, lipid ROS levels were detected using the C11-bodipy probe by FACS. **C** Vitamin K1/K2/K3 exhibited concentration-dependent inhibition of DQ-induced cell death. WT ECs were pre-treated with different concentrations of VK1/2/3 as indicated for 1 h, followed by DQ stimulation for 12 h, and cell viability was assessed. **D** Illustrative images of VK1/2/3 inhibiting DQ-induced cell death. Scale bar = 200 μm. **E** The quantification of cell death from (D) was performed using PI/Hoechst staining and calculated using Image J. **F–N** *WT* mice were subjected to DQ treatment alone ($n = 14$) or pre-treated with MK4 (100 mg/kg, $n = 16$) 24 h and 1 h before DQ treatment. **F** Survival ($n = 16$) was monitored as indicated over time. **G** Representative HE staining of lung and liver sections, as well as PAS staining of kidney sections. The scale bar represents 100 μm. **H–J** Histologic lung, liver, and renal injury scores were determined for each group of mice. A minimum of 10 randomly selected fields were evaluated per mouse. $n = 6$. **K** Representative images of TUNEL staining for assessing cell death. TUNEL staining in green overlapped with DAPI staining in blue. Magnification, ×100; Scale bar = 50 μm. **L–N** TUNEL-positive cells were quantified in 10 randomly selected fields per mouse. $n = 6$.

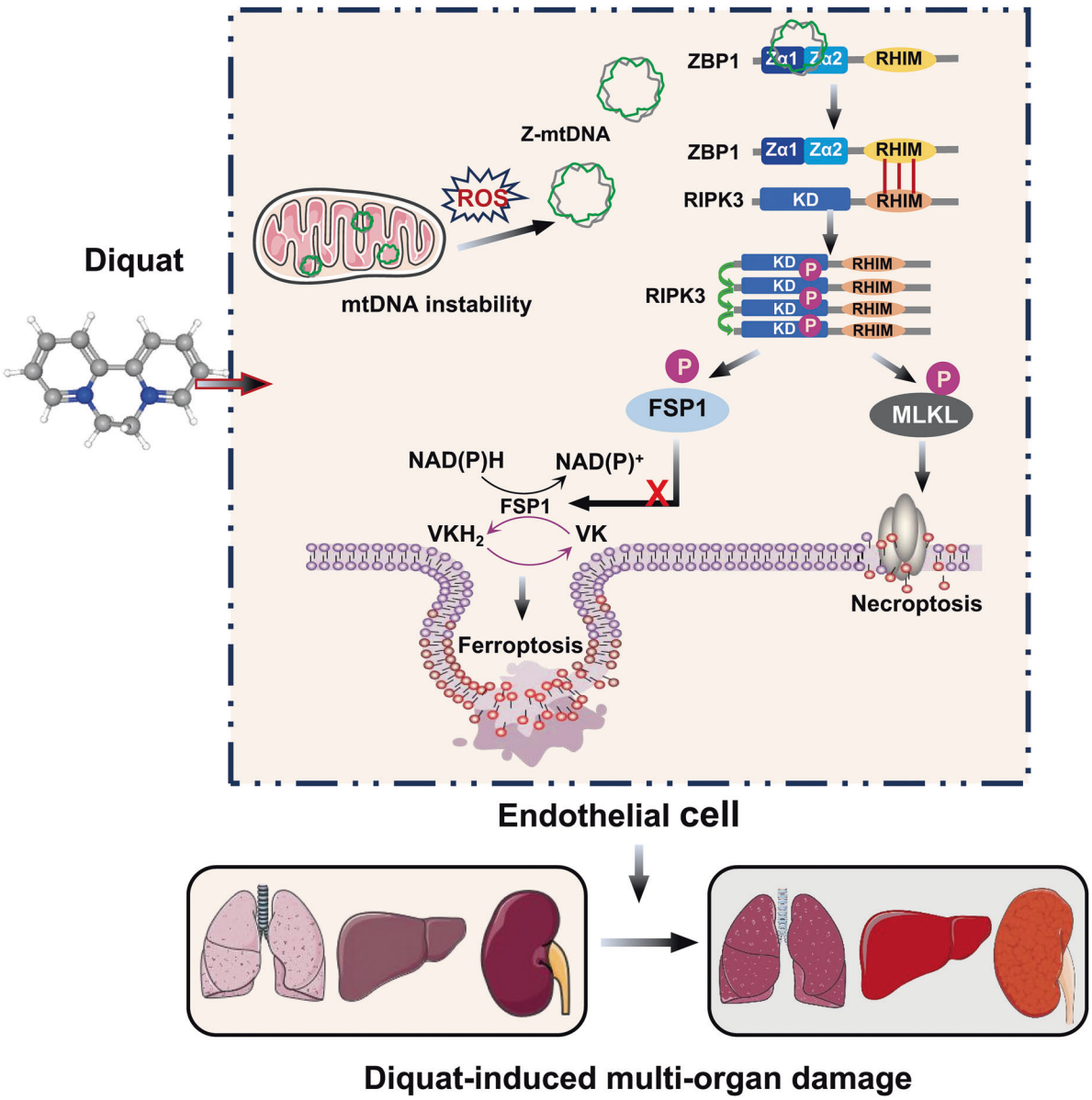

Fig. 8 Schematic model. Z-mtDNA-mediated ZBP1/RIPK3-dependent necroptosis and ferroptosis in endothelial cells as key contributors to the development of organ failure induced by DQ poisoning.

Statistical analyses

Results were represented at least three independently performed experiments. Statistical analysis was performed with Prism software (GraphPad Software, Inc.). The data are expressed as mean ± SD. Group comparisons were conducted using an unpaired *t*-test, and for multiple comparisons, a one-way ANOVA was employed, followed by post hoc Bonferroni correction. Statistical significance was attributed to differences with $^{*}P < 0.05$, $^{**}P < 0.01$, $^{***}P < 0.001$, $^{****}P < 0.0001$.

DATA AVAILABILITY

The datasets used in the current study are available from the corresponding author (YX) upon reasonable request. The mass spectrometry proteomics data have been deposited to the ProteomeXchange Consortium (http://proteomecentral.proteomexchange.org) via the iProX partner repository with the dataset identifier PXD045977. The single-cell sequencing data generated in this study have been deposited in the National Center for Biotechnology Gene Expression Omnibus (https://www.ncbi.nlm.nih.gov/geo/query/acc.cgi?acc=GSE244858).The original western blot data are provided in Supplementary Materials (Original western blots).

REFERENCES

1. Magalhães N, Carvalho F, Dinis-Oliveira RJ. Human and experimental toxicology of diquat poisoning: Toxicokinetics, mechanisms of toxicity, clinical features, and treatment. Hum Exp Toxicol. 2018;37:1131–60.
2. Yu G, Wang J, Jian T, Shi L, Zhao L, Li Y, et al. Case series: diquat poisoning with acute kidney failure, myocardial damage, and rhabdomyolysis. Front Public Health. 2022;10:991587.
3. Meng N, Sun Y, Liu L, Yao D, Gao H, Ma Y, et al. [Clinical features of 86 cases of acute diquat poisoning]. Zhonghua wei zhong bing ji jiu yi xue. 2022;34:301–5.
4. Zhang H, Liu Y, Fang X, Gu L, Luo C, Chen L, et al. Vitamin D(3) protects mice from diquat-induced oxidative stress through the NF-κB/Nrf2/HO-1 signaling pathway. Oxid Med Cell Longev. 2021;2021:6776956.
5. Zhang X, Wang S, Wu Y, Liu X, Wang J, Han D. Ellagic acid alleviates diquat-induced jejunum oxidative stress in C57BL/6 mice through activating Nrf2 mediated signaling pathway. Nutrients. 2022;14:1103.
6. Li X, Zhu J, Lin Q, Yu M, Lu J, Feng J, et al. Effects of curcumin on mitochondrial function, endoplasmic reticulum stress, and mitochondria-associated endoplasmic reticulum membranes in the jejunum of oxidative stress piglets. J Agric Food Chem. 2022;70:8974–85.
7. Carvalho G, Repolês BM, Mendes I, Wanrooij PH. Mitochondrial DNA instability in mammalian cells. Antioxid Rdox Signal. 2022;36:885–905.
8. Xie Y, Hou W, Song X, Yu Y, Huang J, Sun X, et al. Ferroptosis: process and function. Cell Death Differ. 2016;23:369–79.
9. Bock FJ, Tait SWG. Mitochondria as multifaceted regulators of cell death. Nat Rev Mol Cell Biol. 2020;21:85–100.
10. Menger KE, Rodríguez-Luis A, Chapman J, Nicholls TJ. Controlling the topology of mammalian mitochondrial DNA. Open Biol. 2021;11:210168.
11. Menger KE, Chapman J, Díaz-Maldonado H, Khazeem MM, Deen D, Erdinc D, et al. Two type I topoisomerases maintain DNA topology in human mitochondria. Nucleic Acids Res. 2022;50:11154–74.
12. Takaoka A, Wang Z, Choi MK, Yanai H, Negishi H, Ban T, et al. DAI (DLM-1/ZBP1) is a cytosolic DNA sensor and an activator of innate immune response. Nature. 2007;448:501–5.
13. Hubbard NW, Ames JM, Maurano M, Chu LH, Somfleth KY, Gokhale NS, et al. ADAR1 mutation causes ZBP1-dependent immunopathology. Nature. 2022;607:769–75.
14. Jiao H, Wachsmuth L, Wolf S, Lohmann J, Nagata M, Kaya GG, et al. ADAR1 averts fatal type I interferon induction by ZBP1. Nature. 2022;607:776–83.
15. Zhang T, Yin C, Fedorov A, Qiao L, Bao H, Beknazarov N, et al. ADAR1 masks the cancer immunotherapeutic promise of ZBP1-driven necroptosis. Nature. 2022;606:594–602.
16. Lei Y, VanPortfliet JJ, Chen YF, Bryant JD, Li Y, Fails D, et al. Cooperative sensing of mitochondrial DNA by ZBP1 and cGAS promotes cardiotoxicity. Cell. 2023;186:3013–32.e3022.
17. Enzan N, Matsushima S, Ikeda S, Okabe K, Ishikita A, Yamamoto T, et al. ZBP1 protects against mtDNA-induced myocardial inflammation in failing hearts. Circ Res. 2023;132:1110–26.
18. Kuriakose T, Kanneganti TD. ZBP1: innate sensor regulating cell death and inflammation. Trends Immunol. 2018;39:123–34.
19. Jiao H, Wachsmuth L, Kumari S, Schwarzer R, Lin J, Eren RO, et al. Z-nucleic-acid sensing triggers ZBP1-dependent necroptosis and inflammation. Nature. 2020;580:391–5.
20. Dixon SJ, Lemberg KM, Lamprecht MR, Skouta R, Zaitsev EM, Gleason CE, et al. Ferroptosis: an iron-dependent form of nonapoptotic cell death. Cell. 2012;149:1060–72.
21. Stockwell BR. Ferroptosis turns 10: emerging mechanisms, physiological functions, and therapeutic applications. Cell. 2022;185:2401–21.
22. Ahola S, Langer T. Ferroptosis in mitochondrial cardiomyopathy. Trends Cell Biol. 2024;34:150–60.
23. Doll S, Freitas FP, Shah R, Aldrovandi M, da Silva MC, Ingold I, et al. FSP1 is a glutathione-independent ferroptosis suppressor. Nature. 2019;575:693–8.
24. Bersuker K, Hendricks JM, Li Z, Magtanong L, Ford B, Tang PH, et al. The CoQ oxidoreductase FSP1 acts parallel to GPX4 to inhibit ferroptosis. Nature. 2019;575:688–92.
25. Li W, Liang L, Liu S, Yi H, Zhou Y. FSP1: a key regulator of ferroptosis. Trends Mol Med. 2023;29:753–64.
26. Mishima E, Ito J, Wu Z, Nakamura T, Wahida A, Doll S, et al. A non-canonical vitamin K cycle is a potent ferroptosis suppressor. Nature. 2022;608:778–83.
27. Jin DY, Chen X, Liu Y, Williams CM, Pedersen LC, Stafford DW, et al. A genome-wide CRISPR-Cas9 knockout screen identifies FSP1 as the warfarin-resistant vitamin K reductase. Nat Commun. 2023;14:828.
28. Zhang S, Gou S, Zhang Q, Yong X, Gan B, Jia D. FSP1 oxidizes NADPH to suppress ferroptosis. Cell Res. 2023;33:967–70.
29. Lv Y, Liang C, Sun Q, Zhu J, Xu H, Li X, et al. Structural insights into FSP1 catalysis and ferroptosis inhibition. Nat Commun. 2023;14:5933.
30. Chen W, Gullett JM, Tweedell RE, Kanneganti TD. Innate immune inflammatory cell death: PANoptosis and PANoptosomes in host defense and disease. Eur J Immunol. 2023;53:e2250235.
31. Wang Y, Kanneganti TD. From pyroptosis, apoptosis and necroptosis to PANoptosis: a mechanistic compendium of programmed cell death pathways. Comput Struct Biotechnol J. 2021;19:4641–57.
32. Zeng Z, You M, Fan C, Rong R, Li H, Xia X. Pathologically high intraocular pressure induces mitochondrial dysfunction through Drp1 and leads to retinal ganglion cell PANoptosis in glaucoma. Redox Biol. 2023;62:102687.
33. Lin JF, Hu PS, Wang YY, Tan YT, Yu K, Liao K, et al. Phosphorylated NFS1 weakens oxaliplatin-based chemosensitivity of colorectal cancer by preventing PANoptosis. Signal Transduct Target Ther. 2022;7:54.
34. Wang Y, Bin E, Yuan J, Huang M, Chen J, Tang N. Aberrant differentiation of epithelial progenitors is accompanied by a hypoxic microenvironment in the paraquat-injured human lung. Cell Discov. 2023;9:98.
35. West AP, Khoury-Hanold W, Staron M, Tal MC, Pineda CM, Lang SM, et al. Mitochondrial DNA stress primes the antiviral innate immune response. Nature. 2015;520:553–7.
36. Li X, Zhong CQ, Wu R, Xu X, Yang ZH, Cai S, et al. RIP1-dependent linear and nonlinear recruitments of caspase-8 and RIP3 respectively to necrosome specify distinct cell death outcomes. Protein cell. 2021;12:858–76.
37. Szczesny B, Marcatti M, Ahmad A, Montalbano M, Brunyánszki A, Bibli SI, et al. Mitochondrial DNA damage and subsequent activation of Z-DNA binding protein 1 links oxidative stress to inflammation in epithelial cells. Sci Rep. 2018;8:914.
38. Karki R, Kanneganti TD. PANoptosome signaling and therapeutic implications in infection: central role for ZBP1 to activate the inflammasome and PANoptosis. Curr Opin Immunol. 2023;83:102348.
39. Nakamura T, Hipp C, Santos Dias Mourão A, Borggräfe J, Aldrovandi M, Henkelmann B, et al. Phase separation of FSP1 promotes ferroptosis. Nature. 2023;619:371–7.
40. Yang D, Liang Y, Zhao S, Ding Y, Zhuang Q, Shi Q, et al. ZBP1 mediates interferon-induced necroptosis. Cell Mol Immunol. 2020;17:356–68.
41. Wu J, Huang Z, Ren J, Zhang Z, He P, Li Y, et al. Mlkl knockout mice demonstrate the indispensable role of Mlkl in necroptosis. Cell Res. 2013;23:994–1006.
42. He WT, Wan H, Hu L, Chen P, Wang X, Huang Z, et al. Gasdermin D is an executor of pyroptosis and required for interleukin-1β secretion. Cell Res. 2015;25:1285–98.
43. Maelfait J, Liverpool L, Bridgeman A, Ragan KB, Upton JW, Rehwinkel J. Sensing of viral and endogenous RNA by ZBP1/DAI induces necroptosis. EMBO J. 2017;36:2529–43.
44. Bryant JD, Lei Y, VanPortfliet JJ, Winters AD, West AP. Assessing mitochondrial DNA release into the cytosol and subsequent activation of innate immune-related pathways in mammalian cells. Curr Protoc. 2022;2:e372.
45. Xu Y, Ma H, Shao J, Wu J, Zhou L, Zhang Z, et al. A role for tubular necroptosis in cisplatin-induced AKI. J Am Soc Nephrol. 2015;26:2647–58.
46. Chen H, Li Y, Wu J, Li G, Tao X, Lai K, et al. RIPK3 collaborates with GSDMD to drive tissue injury in lethal polymicrobial sepsis. Cell Death Differ. 2020;27:2568–85.

ACKNOWLEDGEMENTS

We are grateful to Prof. Jiahuai Han (Xiamen University), Prof. Wei Mo (Xiamen University) and Ben Lu (Central South University), for experimental materials. Yanfang Xu was supported by Fujian Research and Training Grants for Young and Middle-aged Leaders in Healthcare (2022QNRCYX-XYF), and Outstanding Young Talents Program of the First Affiliated Hospital of Fujian Medical University (YJCQN-A-XYF2021).

AUTHOR CONTRIBUTIONS

YX, HM and JW designed research. KL, JW, SL, GL, KY, YY, YJ, JW, HM performed the mice and molecular experiments. ZC analyzed the single-cell RNA sequencing data. CQZ. conducted the MS data. HM and YX wrote the draft manuscript. YX HM and JW supervised the research and performed writing-review and editing. All authors verified the data and approved the final version of the manuscript.

FUNDING

This work was supported by grants from National Natural Science Foundation of China (U23A20410), Young and Middle-aged Scientific Research Major Project of Fujian Provincial Health Commission (No. 2021ZQNZD004), Joint Funds for the innovation of science and Technology of Fujian province (2021Y9100), Program of the First Affiliated Hospital of Fujian Medical University (YJRC4104), and Fujian Province Finance Project (2020B009).

COMPETING INTERESTS

The authors declare no competing interests.

ETHICS APPROVAL AND CONSENT TO PARTICIPATE

The animal experiments were accomplished in compliance with ethical standards. All animal experiments were approved by the Laboratory Animal Management and Ethics Committee of Fujian Medical University with approved number IACUC FJMU 2022-0886 and were performed in accordance with the "China Guide for the Protection and Use of Laboratory Animals".

ADDITIONAL INFORMATION

Supplementary information The online version contains supplementary material available at https://doi.org/10.1038/s41418-024-01279-5.

Correspondence and requests for materials should be addressed to Jianfeng Wu, Huabin Ma or Yanfang Xu.